Volume 2. Issue 1. 2019

ProClinS Cardiology

Research Article

Open Access

A comparison of the oscillatory shear index on the aortic valve-fibrosa with and without the presence of calcified deposits

Author: Alexander Williams[1], Sharan Ramaswamy[1]*

[1]Department of Biomedical Engineering, Florida International University

***Corresponding author:** Sharan Ramaswamy, Tissue Engineered Mechanics, Imaging and Materials Laboratory (TEMIM Lab), Department of Biomedical Engineering, Florida International University, 10555 W. Flagler Street, EC 2614, Miami, FL 33174, USA. Tel: 305-348-2532, Email: sramaswa@fiu.edu

Received: June 20, 2019; **Accepted:** August 8, 2019; **Published:** August 16, 2019

ABSTRACT

Calcified deposits on the fibrosa side of the aortic heart valve leaflet have been linked to the presence of oscillatory blood flow patterns. This study evaluated the oscillatory shear index (OSI) in a human aortic valve with and without the presence of calcified deposits during the early diastolic phase of the cardiac cycle. The mean OSI in regions which developed calcified deposits was altered negligibly by only 1.6% in comparison to regions which did not calcify, which exhibited a decrease in mean OSI of nearly 36%. Our preliminary results suggest that a noticeable change in oscillatory flow patterns (a decrease in OSI) on the fibrosa-surface will occur during normal rates of valve tissue remodeling with aging. However, when this rate of remodeling is much slower than normal, the OSI will remain relatively unaltered, which may serve as a triggering point for the secretion of a calcified valve extracellular matrix. Clinical monitoring of leaflet fibrosa-OSI may thereby serve as a biomarker for early detection of calcification of the aortic valve, specifically when OSI does not exhibit longitudinal changes.

KEYWORDS: Aortic Valve, Fibrosa, Calcification, Oscillatory shear stress (OSS), Oscillatory shear index (OSI), Tissue Remodeling, Aging

INTRODUCTION

Aortic valve calcification is a predominant cause for aortic insufficiency [1-3]. While there are surgical treatment options available, they have distinct limitations and are generally performed when the native valve is already beyond repair. Therefore, pharmacological management of calcific valve disease during early stages is currently unavailable. Therapeutic discoveries in the treatment of early stages of aortic valve calcification require a fundamental understanding of cellular a mechanism that are regulated by both the local biochemical and biomechanical environments and has been the subject of extensive research.

From a biofluid mechanics standpoint, blood-induced shear stresses across the leaflets have been closely linked to normal and pathological valve tissue remodeling activity [4-10], but spatial and temporal shear stress patterns and magnitudes have yet to be associated with the underlying cell autocrine and paracrine signaling events that regulate the valve extracellular matrix (ECM). For example, as recently demonstrated by Mongkoldhumrongkul et al.[11], fluid-induced shear stresses on both sides of the aortic valve (fibrosa and ventricularis) play critical roles on valvular tissue remodeling. Specifically, it was shown that unidirectional flow regulates valve elastin, while shear stresses resulting from oscillatory flow patterns augment both valve collagen and glycosaminoglycan (GAG) content. Nonetheless, the incidence of pulsatile-flow-induced, low shear, disturbed laminar flow, resulting in oscillatory blood flow on the fibrosa side of aortic valve

leaflets, has been specifically shown to strongly correlate to regions of calcific nodule deposition and aggregation [4,7]. The resulting oscillatory shear stresses (OSS), quantified as an oscillatory shear index (OSI) (Eq. 1), have thus been implicated in valve pathology [6,12]:

$$OSI = 0.5\ x\ \left(1 - \left|\int_0^T WSS\ dt\right| \Big/ \int_0^T |WSS|\ dt\right) \textbf{Equation 1}$$

Where *WSS* represents the blood-induced wall shear stresses over time, we have previously shown that OSS promotes the formation of engineered heart valve tissues [13-15] which included a reporting of a distinct range of OSI values for the conditioning of stem cells for heart valve tissue engineering [16]. However, less understood is the predominant presence of OSS on the aortic valve fibrosa surface and its role, if any, on calcification with aging [7].

Here, we took a computational approach to determine changes in OSS patterns on the human aortic valve fibrosa before and after calcific nodule deposition. In the interest of focusing on a cardiac cycle-specific geometry, in which blood flow oscillations are predominant, we performed simulations and analyses on human aortic heart valve geometry during the early diastolic phase. Note that oscillatory blood flow patterns are predominant when flow disturbances occur during the deceleration phase in late systole as well as in the initial diastolic period [17] .We subsequently compared these findings to regions of the fibrosa that did not develop any pathology.

METHODS

Valve Meshing

No human subjects were recruited in the current study. Instead, computer-aided design (CAD) files of a computed tomography (CT)-image reconstructed human heart valve anatomy from a de-identified patient were commercially available and were thereby purchased (Figure. 1; 82-year old female; Valve-012 - Heart Print catalog, Materialize Inc., Ply mount MI). The position of the valve depicted the early-diastolic, i.e. early closure phase. In the case of the "normal" valve, regions of calcified nodules were computationally removed. The valve geometry without the calcific nodules (Figure.1c) was first discretized utilizing a tetrahedral mesh density ($1.70x10^3$ nodes and $7.73x10^3$ elements, Figure. 1e; ANSYS® Workbench 2016, Ansys Inc., Canonsburg, PA). Next, the original valve with the calcified nodules intact (Figure. 1d) was similarly discretized using a tetrahedral mesh ($4.89x10^4$ nodes, $2.63x10^5$ elements, Figure. 1f; Ansys Inc.). The valves were then fitted within meshed-tubular segments to depict the aorta.

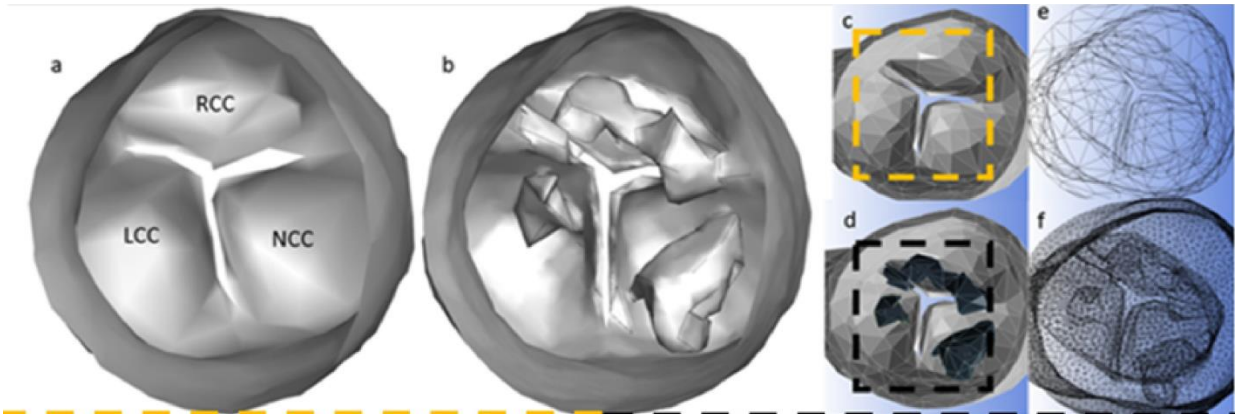

Figure 1: (a) Healthy aortic valve Fibrosa geometryin early diastole, and (b) after calcification. (c)The simulated healthy valve fibrosa geometry and (d) corresponding diseased valve geometry withCT-identified calcified nodules (black) across the leaflets. (e) Mesh of the healthy valve model and (f) the corresponding mesh for the diseased model.

Computational fluid dynamic (CFD) software (Ansys CFX; Ansys Inc.) was used to run simulations to quantify aortic valve WSS. Blood was modelled as a Newtonian fluid with a constant viscosity (3.5 cp) and density (1.06 g/cm^3) [18]. A no-slip boundary condition was applied to the entire geometry for each valve model. Next, pulsatile flow simulations were run for the "normal" and diseased cases with solution convergence criteria of 1×10^{-9} based on previous successfully executed CFD models [14,16]

Inlet and outlet boundary conditions

An aortic flow waveform used in our previous study [16] and originally described by Lotz et al. [19] was prescribed to the inlet while an 80 mm Hg-pressure boundary condition was prescribed to the outlet.

Numerical independence

Independence testing on both valve geometries was carried out to optimize the computational conditions as follows:

Mesh independence

After running a steady state simulation, an optimized tetrahedral mesh density of 1.70x103 nodes and 7.73x103 elements was determined based on the finding that the averaged WSS of the valve and surrounding anatomy was within 5% error of the averaged shear stress of an initial fine mesh (6.67x104 nodes and 3.62x105). Similarly, the diseased valve utilized had an optimized tetrahedral mesh density of 4.89x104 nodes and 2.63x105 elements within 5% error of the averaged shear stress compared to a fine mesh (1.21x105 nodes and 6.69x105 elements)

Courant-Friedrichs-Lewy-time step selection and subsequent

CFD model validation

For both valve geometries utilized, the Courant-Friedrichs-Lewy (CFL) condition was imposed with a Courant number <1 for a time step of 1 ms [20].

In addition, both healthy and diseased valve geometries exhibited a computed average inlet pressure of within 5% of a physiologically realistic value of 120 mm Hg.

Cyclic independence

Cyclic independence was achieved from the 2nd cycle onwards (< 2% error), and hence, the 3rd cycle was selected for post-processing and analysis in both the healthy diseased valve models

RESULTS

Time-averaged shear stress

The spatial distributions of axial time-averaged wall shear stresses (TAWSS) are presented on the healthy valve (Figure. 2a) and diseased valve (Figure. 2c).

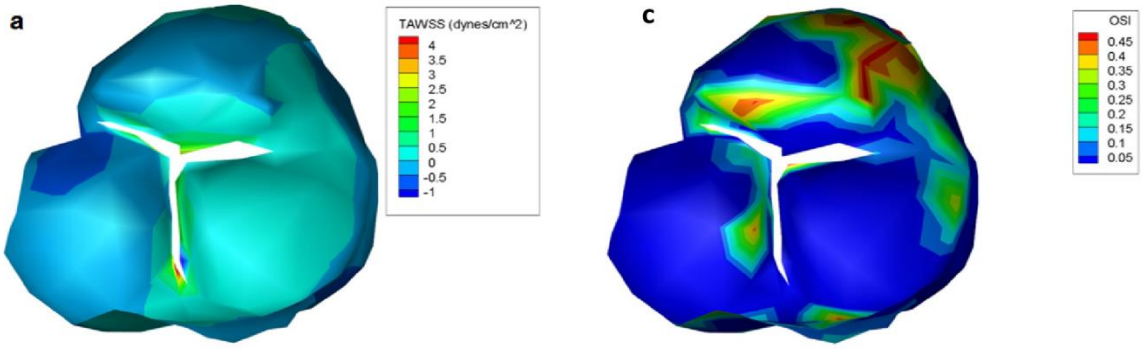

Figure: 2a **Figure: 2c**

Figure 2: "Normal" Valve spatial distribution of (a) mean axial time-averaged wall shear stress (TAWSS; 0.091 dynes/cm2) and Calcified Valve spatial distribution of (c) mean OSI (0.0998) and Calcified Valve spatial distribution.

Healthy valve model

The ventricularis side of the valve had an average (± SEM) axial shear stress of 1.25 ± 0.0195 dynes/cm^2. As expected, the distribution of the shear stresses on the fibrosa side was relatively low in magnitude. The maximum axial shear stresses on the valve were concentrated at the leaflet tips while minimum negative shear stresses were predominantly located across the fibrosa leaflet bellies. The mean fibrosa axial stress value of the valve was 0.091± 0.067 dynes/cm^2.

Calcified valve model

The ventricularis side of the valve exhibited an average axial shear stress (± SEM) of 1.95 ± 0.001 dynes/cm². Maximum shear stresses were, as in the case of the healthy valve, located at the leaflet tips. Minimum negative stresses were concentrated at the surface of the leaflet bellies (Figure. 2c). The average fibrosa axial shear stress value of the valve was 0.32 ± 0.004 dynes/cm².

Oscillatory shear index

The spatial distributions of OSI were computed for the healthy valve (Figure. 2b) and diseased valve (Figure. 2d) cases; averaged OSI values in regions A1 – A4 were subsequently summarized (Table 1). Regional distribution of OSI on the aortic valve leaflet surfaces (ventricularis vs. fibrosa) before and after calcification can be summarized as follows:

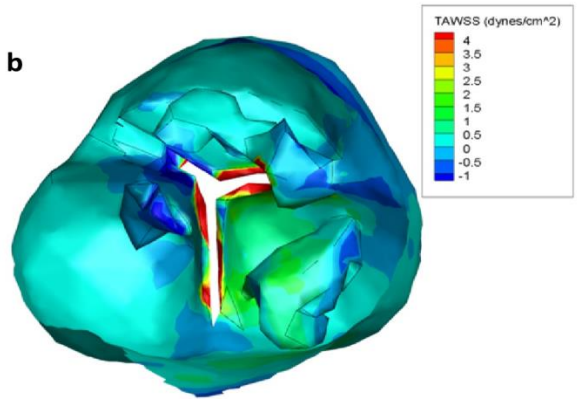

Figure: 2b

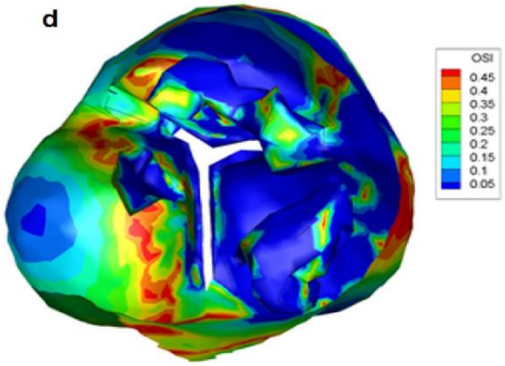

Figure: 2d

Figure 2: "Normal" Valve spatial distribution of (b) mean axial time-averaged wall shear stress (TAWSS; 0.323 dynes/cm²). "Normal" Valve spatial distributions of (d) mean OSI (0.1557).

Calcified Region	A1	A2	A3	A4
Mean±SEM	0.088±0.0721	0.103±0.056	0.0894±0.015	0.14±0.0622

Table 1: OSI on cusp-designated areas of the valve fibrosa (A1-A4) for each region

Healthy valve model

OSI on the ventricularis side of the valve was negligible (mean OSI = 0.003; range: 0 – 0.1311). The OSI on the fibrosa side was much higher with leaflet area-averaged OSIs ranging from 0.060 to 0.147 (mean OSI = 0.103).

Calcified valve model

Similar to the healthy valve, the OSI on the ventricularis side of the calcified valve (mean OSI =0.010; range 0 – 0.4389) was substantially lower than that of the fibrosa. The leaflet area-averaged OSIs across the calcified valve fibrosa ranged from 0.051 to 0.211 (mean OSI = 0.156).

Regions that developed calcification

Regions that developed calcification had OSIs ranging from 0.06 to 0.108 with the collective OSI of these regions (area A3, Figure. 1h) exhibiting an overall Mean OSI ± SEM of 0.089 ± 0.015 (Table 1). The corresponding regions of A3 on the healthy valve were found to have OSIs ranging from 0.009 to 0.0232 with the mean OSI of these regions (area A1, Figure. 1g) being 0.088 ± 0.0721 (Table 1). The unaffected regions surrounding A3 exhibited OSIs ranging from 0.0267 to 0.2411with the mean OSI of these regions (area A4, Figure. 1h) being 0.14 ± 0.0622 (Table 1). Corresponding regions for A4 on the healthy valve had OSIs ranging from 0.05 to 0.215 with the mean OSI of these regions (area A2, Figure. 1g) being 0.103 ± 0.056 (Table 1).

Calcified Region	A1	A2	A3	A4
Mean±SEM	0.088±0.0721	0.103±0.056	0.0894±0.015	0.14±0.0622

Table 1: OSI on cusp-designated areas of the valve fibrosa (A1-A4) for each region, Note that A3 and A4 are the calcified and unaffected regions of the calcified valve (Figure. 1h) respectively, while A1 and A2 are the corresponding spatial locations to A3 and A4 in the "normal" valve (Figure. 1g). Mean ± SEM is provided for each area. A slight shift in OSI (1.6%) occurred between the mean OSIs of A1 and A3.

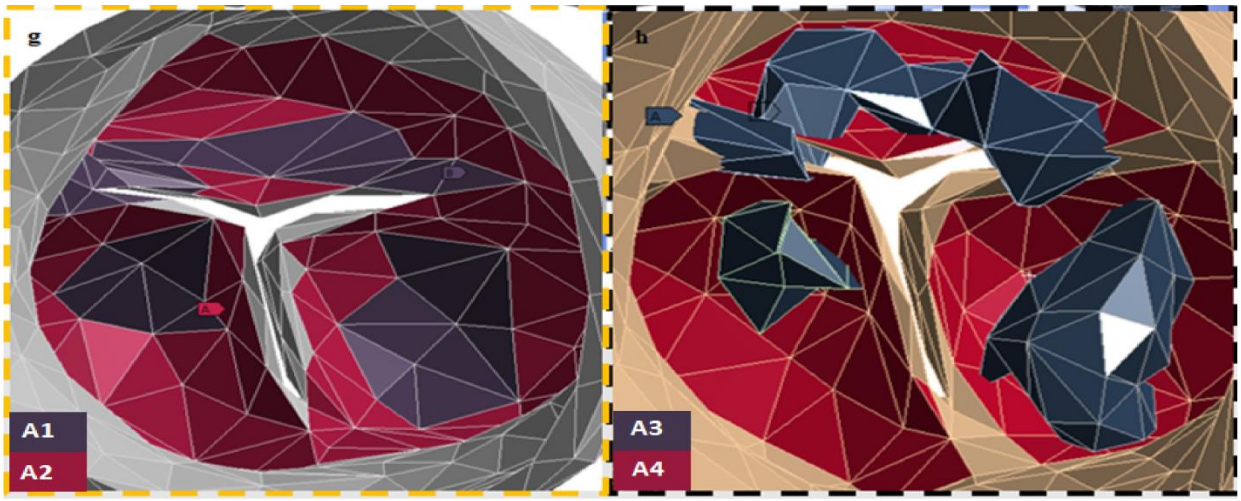

Figure: 1g **Figure: 1h**

Areas of interest (A1, A2, A3, A4): Region A1 (black) and A2 (red) are from (g) the healthy valve geometry, while the same regions are labeled as A3 (black) and A4 (red) on (h) the diseased valve, respectively. Note that region A3 contains plaque deposits while region A4 remained free of calcific deposits. The calcified deposits on the diseased aortic valve necessitated a different mesh topology and density compared to the "normal" valve. As a result, the regions A1 vs A3 and A2 vs A4 do not enable exact spatial correspondence, but rather provide a rough approximation for comparative purposes. The spatial size of the calcific regions (A3) on the diseased valve (h,295.1 mm2). The regions on the diseased valve that were free of calcific deposits (area A4, red) were found to surround the A3-regions (637.9 mm2). Corresponding regions A1 and A2 to A3 and A4 respectively, before the onset of disease, i.e., the "normal" valve, were also determined (g, A1: 243.1 mm2, A2: 660.7 mm2)

Percent (%) change in OSI

The percent decrease in OSI (Table 2) in the region of the calcified valve (A3) compared to the same location when it was not diseased (A1) was found to be marginal (1.59%). On the other hand, the regions that remained unaffected by calcification on both valves (A2, A4) had a much more substantial decrease in OSI of 35. 9%.

%Change (Mean A1 & Mean A3)	%Change (Mean A2 & Mean A4)	%Change in NCC	%Change in RCC	%Change in LCC
1.59(SD: 1.12, SEM:0.80)	35.9 (SD: 25.4, SEM:18)	34.8 (plaque %: 38.2)	11.0 (plaque %: 39.8)	688.0 (plaque %: 5.23)

Table 2: Percent (%) change in mean OSI of cusp-designated regions (non-coronary cusp, NCC; right-coronary cusp, RCC and left-coronary cusp, LCC) and in mean OSI across distinct valvular cusps. As shown in Table 2, there was a markedly low percentage change between the mean OSIs of A1 and A3 (1.6 %) on the valve surfaces that eventually developed calcified deposits. On the other hand, regions that did not progress to disease states were found to have a much larger mean percent OSI change of ~ 36% (between regions A2 and A4).

DISCUSSION

Our long-standing understanding of sites of atherosclerosis in vascular disease with regions of flow disturbance or blood flow oscillations may also be applicable in valvular diseases. Accordingly, here we investigated the regional changes in a human aortic valve oscillatory flow distribution (OSI) before and after calcified deposits. Axial TAWSS results from affected and unaffected regions of both valve models (Figure. 2a, 2c) revealed that non-unidirectional flow dominated

across the aortic valve fibrosa surfaces, thereby confirming that the native valve environments were subjected to OSS. The computed WSS on the surfaces of human patient-specific geometry derived aortic valve model that were simulated here had values in the range of -5.94 dynes/cm2 to 54.7 dynes/cm2, which are consistent within values previously reported in the literature [4,5,11,21] and with relatively lower WSS found on the fibrosa side (mean WSS: 0.091 dynes/cm2) compared to the ventricularis side (mean WSS:1.25 dynes/cm2).

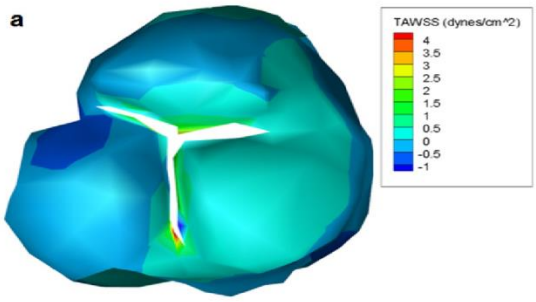

Figure: 2a

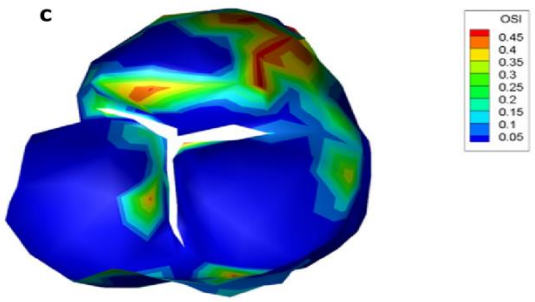

Figure: 2c

Figure 2: "Normal" Valve spatial distribution of (a) mean axial time-averaged wall shear stress (TAWSS; 0.091 dynes/cm2) and Calcified Valve spatial distribution of (c) mean OSI (0.0998) and Calcified Valve spatial distribution.

In agreement with previous investigations [4,21,22], the non-coronary cusp (NCC) and right coronary cusp (RCC) of the fibrosa were found to be most susceptible to calcification in the human valve geometry that was used here (Materialise Inc.). Moreover, of particular interest, regions susceptible to high calcification had only marginal changes in the OSI (healthy tissue area, A1: Mean ± SEM OSI: 0.088 ± 0.072 and same tissue area A1, after calcification, i.e., A3: Mean ± SEM OSI: 0.089 ± 0.015), resulting in a change in OSI of only 1.59%. Conversely, regions of the aortic valve that did not get calcified, i.e. A2 and later A4, exhibited a rather substantial change in OSI of nearly 36%. These findings suggest that relative changes in OSI or lack thereof between healthy and valve pathologies could potentially be used to predict regions on the valve fibrosa prone to calcification. Specifically, we speculate that in situations where the rate of valve matrix remodeling slows down, a change in OSI is unlikely with aging. Based on the results found herein, that calcified regions on the aortic valve simulated exhibited marginal changes in OSI (1.6%) compared to regions on the valve that remained unaffected by calcified deposits (36%), we conclude that insufficient rates of valve tissue remodeling or marginal longitudinal changes in valve structure, could serve as a trigger for aortic valve calcification. Aortic valve calcification is strongly correlated with the aging process. Hence, we speculate that longitudinal tissue remodeling changes in valve structure will affect regional, i.e., fibrosa aortic valve hemodynamics, thereby leading OSI changes. One scenario could be that normal valve tissue remodeling, i.e., changes in valve elastin, collagen and/or glycosaminoglycans (GAGs) which could affect the overall curvature of the leaflet tissues; conversely lack of sufficient tissue remodeling would retain the valve structure and hence the fibrosa OSI, which could serve as a trigger for onset of valve pathology later in life.

Limitations:

The findings in this brief manuscript are very preliminary and contain two major limitations in the approaches. Firstly, a single patient's valve was analyzed before and after calcification. In other words, we caution the reader that a major limitation of the current study it is based on only an n =1 pre/post patient data-set. The intent of the current manuscript was primarily to introduce the concept of changes in OSI with valve tissue pathology and that this would initiate an interest in the scientific community to investigate flow-based biomarkers that could be monitored for aortic valve calcification. Secondly, the flow physics in a pulsatile flow model without accounting for valve leaflet motion was simulated during the early-diastolic, closing phase of the valve. However, oscillatory effects are relatively high during the early diastolic phase [16].Moreover, the overall trend that negligible longitudinal changes in OSI co-related with regions of calcified plaque deposits on the valve is, nonetheless, likely to hold. Finally, as our focus here was primarily on computational quantification of OSI between a healthy and calcified aortic valve, another limitation currently is that assessment of specific valve biochemistry needs to be experimentally identified and correlated with the computed OSI values. In conclusion, we present a new interpretation of OSI in the context of aortic valve calcification. In cases of *in vitro* tissue engineering protocols, a targeted value of OSI may be prescribed to promote *de novo* tissue growth as we previously described [16]. However, when the OSI remains relatively unchanged, this may be suggestive of an absence of or an insufficient rate of valve ECM remodeling, which could lead to a triggering point for valve calcification. Therefore, in

addition to the OSI itself, *a change in the leaflet, fibrosa-side OSI with aging, or specifically, a lack thereof* may serve useful as a bio-marker for the early detection of aortic valve calcification. For example, echocardiography, computed tomography and magnetic resonance imaging techniques are utilized to obtain either structural and/or functional, i.e. flow-based information for the aortic valve. These image-datasets between any two given patient visits could be discretized, along with the application of relevant flow/pressure boundary conditions to perform subsequent CFD simulations, thereby yielding a % mean change in OSI value for interpretation of the valve's susceptibility to future calcification.

ACKNOWLEDGEMENTS:

The authors gratefully acknowledge funding support through a Coulter SEED Grant, Department of Biomedical Engineering, College of Engineering and Computing, Florida International University, Miami, FL. The authors also thank the writing center at the City University of New York, New York, NY for their assistance in proofreading the manuscript.

DECLARATIONS:

Conflicts of Interest: Author, Alexander Williams and Author, Sharan Ramaswamy, declare that they have no conflict of interest.
Human Studies: No human studies were carried out by the authors for this study.
Animal Studies: No animal studies were carried out by the authors for this study.

REFERENCES

1. Peeters FECM, Meex SJR, Dweck MR, Aikawa E, Crijns HJGM, et al. Calcific aortic valve stenosis: hard disease in the heart: A biomolecular approach towards diagnosis and treatment. Eur Heart J. 2018; 39: 2618-2624.
2. Stewart BF, Siscovick D, Lind BK, Gardin JM, Gottdiener JS, et al. Clinical factors associated with calcific aortic valve disease. Cardiovascular Health Study. J Am Coll Cardiol. 1997; 29: 630–634.
3. Wirrig EE, Yutzey KE. Transcriptional regulation of heart valve development and disease. Cardiovasc Pathol. 2011; 20: 162–167.
4. Yap CH, Saikrishnan N, Tamilselvan G, Yoganathan AP. Experimental measurement of dynamic fluid shear stress on the aortic surface of the aortic valve leaflet. Biomech Model Mechanobiol. 2012; 11: 171–182.
5. Yap CH, Saikrishnan N, Yoganathan AP. Experimental measurement of dynamic fluid shear stress on the ventricular surface of the aortic valve leaflet. Biomech Model Mechanobiol. 2012; 11: 231–244.
6. Cao K, BukaČ M, Sucosky P. Three-dimensional macro-scale assessment of regional and temporal wall shear stress characteristics on aortic valve leaflets. Comput Methods Biomech Biomed Engin. 2016; 19: 603–613.
7. Sun L, Rajamannan NM, Sucosky P. Defining the role of fluid shear stress in the expression of early signaling markers for calcific aortic valve disease. PLoS One. 2013; 8: e84433.
8. Engelmayr GC, Sales VL, Mayer JE, Sacks MS. Cyclic flexure and laminar flow synergistically accelerate mesenchymal stem cell-mediated engineered tissue formation: Implications for engineered heart valve tissues. Biomaterials. 2006; 27: 6083–6095.
9. Ge L, Sotiropoulos F. Direction and Magnitude of Blood Flow Shear Stresses on the Leaflets of Aortic Valves: Is There a Link with Valve Calcification? J Biomech Eng. 2010; 132: 014505.
10. Zhang Z, Yuan L, Lee PD, Jones E, Jones JR. Modeling of time dependent localized flow shear stress and its impact on cellular growth within additive manufactured titanium implants. J Biomed Mater Res Part B Appl Biomater. 2014; 102: 1689–1699.
11. Mongkoldhumrongkul N, Latif N, Yacoub MH, Chester AH. Effect of Side-Specific Valvular Shear Stress on the Content of Extracellular Matrix in Aortic Valves. Cardiovasc Eng Technol. 2016; 9: 151-157.
12. Cao K, Sucosky P. Computational comparison of regional stress and deformation characteristics in tricuspid and bicuspid aortic valve leaflets. Int J Numer Method Biomed Eng. 2017; 33: 2798.
13. Rath S, Salinas M, Villegas AG, Ramaswamy S. Differentiation and Distribution of Marrow Stem Cells in Flex-Flow Environments Demonstrate Support of the Valvular Phenotype. PLoS One. 2015; 10: e0141802.
14. Salinas M, Rath S, Villegas A, Unnikrishnan V, Ramaswamy S. Relative Effects of Fluid Oscillations and Nutrient Transport in the In Vitro Growth of Valvular Tissues. Cardiovasc Eng Technol. 2016; 7: 170–181.
15. Salinas M, Ramaswamy S. Computational simulations predict a key role for oscillatory fluid shear stress in de novo valvular tissue formation. J Biomech. 2014; 47: 3517–3523.
16. Williams A, Nasim S, Salinas M, Moshkforoush A, Tsoukias N, et al. A "sweet-spot" for fluid-induced oscillations in the conditioning of stem cell-based

engineered heart valve tissues. J Biomech. 2017; 65: 40–48.
17. Ku DN, Giddens DP. Laser Doppler anemometer measurements of pulsatile flow in a model carotid bifurcation. J Biomech. 1987; 20: 407–421.
18. Pinkowski A, Lilienblum W. A Hydrodynamic Approach to Cancer. bioRxiv. 2015; 014696.
19. Lotz J, Meier C, Leppert A, Galanski M. Cardiovascular Flow Measurement with Phase-Contrast MR Imaging: Basic Facts and Implementation. RadioGraphics. 2002; 22: 651–671.
20. Wendell DC, Samyn MM, Cava JR, Ellwein LM, Krolikowski MM, et al. Including aortic valve morphology in computational fluid dynamics simulations: initial findings and application to aortic coarctation. Med Eng Phys. 2013; 35: 723–735.
21. Sacks MS, Yoganathan AP. Heart valve function: a biomechanical perspective. Philos Trans R Soc Lond B Biol Sci. 2007; 362: 1369–1391.